Simulation of runaway electron generation in the Day-0 scenario of DTT

Fusion Engineering and Design 223 (2026) 115588

Contents lists available at ScienceDirect

Fusion Engineering and Design

journal homepage: www.elsevier.com/locate/fusengdes

Simulation of runaway electron generation in the Day-0 scenario of DTT☆

Enrico Emanuelli [a,b,*], Francesco Vannini [c], Matthias Hoelzl [c], Nina Schwarz [d], Eric Nardon [e], Vinodh Bandaru [f], Daniele Bonfiglio [g,h], Artur Kryzhanovskyy [g], Giuseppe Ramogida [b,i,j], Fabio Subba [a], JOREK Team[1]

[a] NEMO Group, Dipartimento Energia, Politecnico di Torino, Corso Duca degli Abruzzi 24, Torino, 10129, Italy
[b] DTT S.C.a.r.l., Via Enrico Fermi 45, Frascati, 00044, Italy
[c] Max Planck Institute for Plasma Physics, Boltzmannstr. 2, Garching bei München, 85748, Germany
[d] ITER Organization, Route de Vinon-sur-Verdon, Saint-Paul-lez-Durance, Cedex, 13067, France
[e] CEA, IRFM, F-13108 Saint-Paul-lez-Durance, France
[f] Indian Institute of Technology Guwahati, North Guwahati, Assam, 781039, India
[g] Consorzio RFX, Corso Stati Uniti 4, Padova, 35127, Italy
[h] CNR-ISTP, Corso Stati Uniti 4, Padova, 35127, Italy
[i] ENEA, Via Enrico Fermi 45, Frascati, 00044, Italy
[j] Università della Tuscia, Via Santa Maria in Gradi 4, Viterbo, 01100, Italy

ARTICLE INFO

Keywords:
Runaway electrons
DTT
Disruptions
JOREK

ABSTRACT

Formation of Runaway electrons (REs) during tokamak disruptions is a significant challenge in fusion research, as they can locally damage the plasma-facing components by applying thermal loads of tens of MJ per square meter, possibly leading to significant melting. This work investigates the current quench phase of disruptions and the likelihood of RE generation and multiplication in the Day-0 scenario (plasma current $I_p = 2$ MA) of the Divertor Tokamak Test (DTT), using the non-linear magnetohydrodynamic code JOREK. Our results from 2D (toroidally symmetric) simulations indicate that, in this initial low-current scenario, RE generation is minimal to negligible when the impurities injected through disruption mitigation systems are adequately limited. This suggests that DTT's early operational phase poses a low RE risk, contributing to operational safety in this regard before transitioning to full power scenarios ($I_p = 5.5$ MA). In addition to providing an initial RE safety benchmark for DTT, this study lays the groundwork for further research at higher operational currents and for the estimation of heat loads caused by RE beams on plasma-facing components, essential for guiding the design and strategic placement of mitigation elements such as sacrificial limiters.

1. Introduction

The operation of magnetic confinement fusion devices, such as tokamaks, involves significant challenges, among which plasma disruptions stand out due to their potential to cause severe structural damage and shorten the lifespan of such machines [1,2]. Although advanced control systems are designed to stabilize the plasma, unforeseen failures or magnetohydrodynamic (MHD) instabilities can still trigger abrupt disruptions. These events release the majority of the plasma's thermal and magnetic energy over a millisecond timescale, subjecting plasma-facing components (PFCs) and structural elements to intense mechanical and thermal loads [2], which may become unacceptable for larger devices such as ITER [3] or EU-DEMO [4]. Therefore, disruptions of any kind must either be avoided or mitigated in large tokamak devices.

An effective mitigation technique to reduce their impact on the reactor involves injecting large amounts of deuterium and impurities into the plasma when a disruption is predicted. Impurities radiatively cool the plasma, which releases a substantial portion of its thermal and magnetic energy on a millisecond timescale. This controlled cooling can help reduce the mechanical stresses on the structure by limiting the vertical forces exerted on the wall [5]. The abrupt increase in plasma resistivity caused by the low temperatures found at the end of the thermal quench (TQ) causes the plasma current to decay during the current quench (CQ), releasing the stored magnetic energy and effectively bringing the discharge to an end. However, the self-induced toroidal electric field caused by the CQ can accelerate a portion of the electron population to relativistic speeds, leading to the formation of

☆ This article is part of a Special issue entitled: 'SOFT 2024' published in Fusion Engineering and Design.

* Corresponding author at: NEMO Group, Dipartimento Energia, Politecnico di Torino, Corso Duca degli Abruzzi 24, Torino, 10129, Italy.
E-mail address: enrico.emanuelli@polito.it (E. Emanuelli).

[1] See author list of M. Hoelzl et al 2024 Nucl. Fusion 64 112016.

https://doi.org/10.1016/j.fusengdes.2025.115588
Received 17 January 2025; Received in revised form 11 August 2025; Accepted 7 December 2025

a population of runaway electrons (REs) [6,7]. Through the avalanche mechanism, REs can multiply and form beams that can carry a significant fraction of the pre-disruption plasma current, with the potential avalanche gain scaling exponentially with the plasma current [7]. The uncontrolled interaction of such a high runaway current with PFCs can cause severe local damage, including significant surface melting and substantial damage to the underlying substrate structures [2,8,9].

The Divertor Tokamak Test (DTT) [10,11], a facility currently under construction in Italy, is intended as a testbed to address specific challenges in fusion energy, particularly those related to different plasma and exhaust scenarios. Using a significant amount of external heating power (up to 45 MW delivered to the plasma), DTT aims to replicate the level of divertor heat loads foreseen in ITER and EU-DEMO [11]. This will allow DTT to test and develop robust strategies and technologies, such as magnetic configurations involving a large divertor wetted area or the use of liquid metal PFCs, applicable to the next generation of fusion reactors. Despite operating at lower plasma currents compared to larger tokamaks, DTT can still face significant RE-related risks. Although the potential for RE formation is more pronounced in the full power scenario with a nominal plasma current $I_p = 5.5$ MA, it cannot be overlooked even in lower current scenarios. This is particularly evident from previous observations in JET, where a plasma current comparable to that of the Day-0 scenario of DTT ($I_p = 2$ MA) resulted in RE generation and subsequent wall damage [8]. These findings underscore the critical importance of understanding and mitigating RE risks in all operational phases of DTT. In particular, gaining insights into RE dynamics in the Day-0 scenario of DTT is crucial for ensuring that REs remain at negligible levels during early operations and informing the progressive scale-up to the full power scenarios.

This work aims to assess the risks of RE generation in the Day-0 scenario of DTT. To achieve this, we simulate plasma disruptions using the non-linear MHD code JOREK [12,13], coupled with the vacuum-field code STARWALL [14,15]. 2D simulations (i.e., toroidally symmetric) are carried out to systematically study the formation of REs in the CQ phase for different initial RE seed currents and impurity levels, offering comprehensive insights into the impact of REs under early operational conditions.

The paper is organized as follows: Section 2 describes the models and methods, including the most important details of the JOREK code, of the artificial thermal quench (ATQ) procedure, and of the DTT Day-0 scenario. Section 3 presents the results of the simulations, highlighting the effects of various disruption scenarios and initial RE seeds on the generation of REs. Finally, in Section 4 we draw the conclusions of this work.

2. Models and methods

The analysis of RE generation in the Day-0 operational phase of DTT requires an advanced, self-consistent simulation approach to accurately capture plasma dynamics and interactions with surrounding conducting structures. We employ the non-linear MHD code JOREK [12,13] in conjunction with the vacuum-field simulation code STARWALL [14,15]. This section highlights the key features of JOREK and STARWALL, as well as the ATQ procedure used to replicate the start of the disruption, enabling a focused investigation of the CQ phase and the associated RE avalanche growth. Additionally, we outline relevant details of DTT and its Day-0 scenario, along with the parameter space explored to examine RE formation.

JOREK is a well-established code for modeling non-linear MHD phenomena in magnetically confined fusion devices, able to handle the complex dynamics associated with plasma instabilities, disruptions, and RE formation and interaction with MHD modes. While various full MHD models are available in JOREK, we consider here a reduced MHD model, in order to reduce computational costs while still being able to capture the essential dynamics of interest. Indeed, since we are focusing on axisymmetric dynamics, reduced MHD and full MHD are fully equivalent. This model is obtained by expressing the magnetic field ($\boldsymbol{B}$), electric field ($\boldsymbol{E}$) and plasma fluid velocity ($\boldsymbol{v}$) as

$$\begin{aligned} \boldsymbol{B} &= \frac{1}{R}\nabla\psi \times \hat{e}_\phi + \frac{F_0}{R}\hat{e}_\phi, \\ \boldsymbol{E} &= -F_0\nabla u - \frac{1}{R}\frac{\partial\psi}{\partial t}\hat{e}_\phi, \\ \boldsymbol{v} &\approx -R\nabla u \times \hat{e}_\phi, \end{aligned} \tag{1}$$

where R is the major radial coordinate, ψ is the poloidal magnetic flux, $\hat{e}_\phi$ is the unit vector in the toroidal direction, F_0 is a constant in space and time describing the intensity of the vacuum toroidal magnetic field $B_{\phi,0}$ ($F_0 = R_0 B_{\phi,0}$, R_0 being the major radius of the plasma axis) and u is the velocity stream function, defined as the electric scalar potential Φ divided by F_0. The full details of the reduced MHD model and the numerical schemes used in JOREK are described in [12,16]. JOREK includes an RE fluid model coupled with the MHD equations [17], which treats REs as a distinct fluid population within the plasma. This model self-consistently couples the RE population with the evolving plasma current and electric fields, thus capturing the feedback effects between REs and the bulk plasma. In this work, when included, REs are initialized through an initial RE seed current that is already present at the beginning of the simulations. This initial seed is representative of the primary formation mechanisms of REs, such as hot-tail or Dreicer. A secondary volumetric source is the avalanche mechanism, whereby REs multiply through collisions with background electrons, potentially leading to substantial RE currents during the CQ phase [18]. Full details of this model and its coupling with MHD equations can be found in [19]. This model has already been successfully applied to simulate RE beam generation and termination events in JET [20], ITER [21–24] and EU-DEMO [25]. Specifically, [23] focuses on 2D predictive simulations with extensive parameter scans, while the 2D predictive simulations of [24] emphasize the importance of free-boundary simulations to accurately capture REs avalanching correctly. Additionally, [25] investigates 2D predictive RE formation and 3D termination simulations, which offer estimates for RE beam amplitudes at different impurity contents and assess the effectiveness of a sacrificial limiter for machine protection. In the present study, the JOREK simulations were performed with an axisymmetric 2D reduced MHD model. The RE beam formation is studied in the absence of non-axisymmetric perturbations as an upper estimate in the absence of stochastic fields. Due to their complexity and computational costs, these simulations will be addressed in future work.

Table 1 summarizes the main parameters used in all the simulations performed in this work, unless explicitly stated otherwise. Other assumptions used in this work include the adoption of a single-fluid representation of the background plasma, assuming that it is described by a single temperature and that the electron and ion temperatures are equal ($T = T_i + T_e = 2T_e$). This allows us to capture the overall energy dynamics while reducing the computational cost of the simulations. Additional simplifications that significantly reduce computational costs are setting the parallel velocity of the background ions and impurities and the diamagnetic drift velocities to 0 and neglecting the presence of neutral particles. In practice, having $v_\parallel = 0$ and $v_{\text{dia}} = 0$ transforms the last equation in (1) to $\boldsymbol{v} = -R\nabla u \times \hat{e}_\phi$. Fixed boundary conditions (BCs) are applied to all fluid variables, while BCs of the poloidal magnetic flux ψ and the total toroidal current density j are determined through coupling of JOREK with the resistive wall code STARWALL. This allows us to limit the computational domain to the plasma region. The details of the coupling can be found in [15]. Implementing dynamical boundary conditions through STARWALL enables us to evolve plasma dynamics together with the currents flowing in the physical structures of DTT, providing a realistic representation of the current quench phase and RE dynamics under experimental conditions. Fig. 1 shows a 2D sectional view in the R-Z plane of the active and passive DTT conducting structures imported into STARWALL. The inner shell of the vacuum vessel was modeled using an axisymmetric thin wall (orange

Table 1
Physical parameters used in all the simulations (unless stated otherwise). η_e is the plasma resistivity, while $\chi_\parallel$ and $\chi_\perp$ denote the parallel and perpendicular thermal diffusivities, respectively. D is the particle diffusivity, which is isotropic for the thermal plasma and impurities, but split between parallel and perpendicular components for REs ($D_{\parallel,RE}$ and $D_{\perp,RE}$, respectively). The very high value for $D_{\parallel,RE}$ is used to model the parallel transport of REs, mimicking their fast parallel advection. This optimal value was found through extensive tests with the JOREK RE fluid model, and it does not cause any significant numerical perpendicular diffusion [19]. Instead, the relatively small value of $D_{\perp,RE}$ is intended to provide numerical stability [21].

Parameter		Dependency	Value
η_e	$T_e < 500\,\text{eV}$	Spitzer $\propto T_e^{-3/2}$	$\eta_e = \eta_{e,\text{Sp}}$
	$T_e \geq 500\,\text{eV}$	Constant	$\eta_e = \eta_e^{\min} = \eta_{e,\text{Sp}}(@500\,\text{eV})$
$\chi_\parallel$	$T_e < 350\,\text{eV}$	Spitzer-Harm $\propto T_e^{5/2}$	$\chi_\parallel = \chi_{\parallel,\text{SH}}$
	$T_e \geq 350\,\text{eV}$	Constant	$\chi_\parallel = \chi_\parallel^{\max} = \chi_{\parallel,\text{SH}}(@350\,\text{eV})$
$\chi_\perp$		Profile	$\chi_{\perp,\text{core}} = 2\,\text{m}^2/\text{s}$
D		Constant	$1.23\,\text{m}^2/\text{s}$
$D_{\parallel,RE}$		Constant	$1.83 \times 10^9\,\text{m}^2/\text{s}$
$D_{\perp,RE}$		Constant	$1.83 \times 10^{-2}\,\text{m}^2/\text{s}$

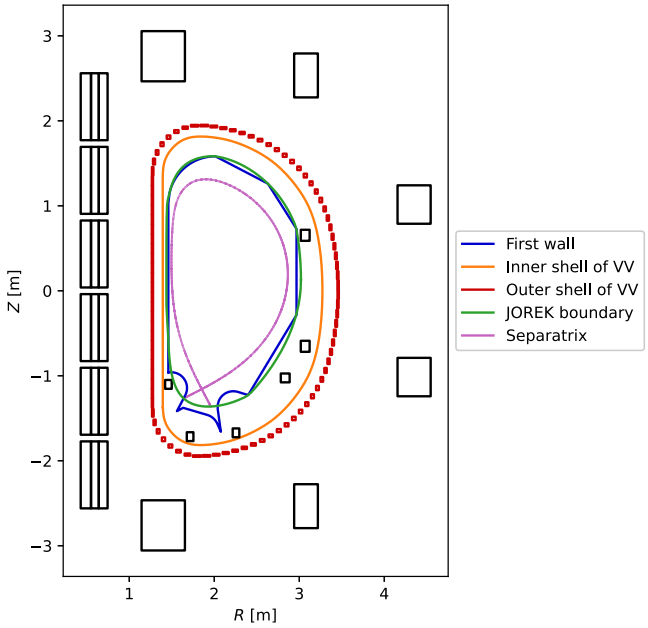

Fig. 1. 2D sectional view in the R-Z plane showing the active and passive conducting structures of DTT discretized in STARWALL. The inner and outer shells of the vacuum vessel are represented by an axisymmetric thin wall (orange line) and through filaments (small red rectangles), respectively. The poloidal field coils, in-vessel coils and central solenoid are depicted in black. The first wall is shown as a blue line, with the JOREK computational boundary (green line) closely adherent to it, avoiding sharp discontinuities. For reference, the separatrix in this SN Day-0 scenario of DTT is shown in pink.

line), whereas the outer shell was modeled using toroidal filaments (red rectangles). The other conductive structures include the poloidal field coils, the central solenoid, and the in-vessel coils. The figure also shows the JOREK computational boundary (green line), which has been chosen to be as adherent as possible to the first wall (blue line), to avoid the sharp discontinuities of the latter. For reference, the separatrix of this SN Day-0 scenario of DTT is also displayed in pink. The vacuum vessel (VV) is made of stainless steel and the inner and outer shells have a resistivity $\eta_w = 0.75\ \mu\Omega\text{m}$ and a thickness $d_w = 15$ mm.

To simulate the conditions of a plasma disruption and analyze RE formation, we implement an artificial thermal quench (ATQ) within JOREK, as successfully done in the past in other tokamak environments [5,21,24–26]. Although JOREK can simulate the TQ resulting from massive material injection self-consistently [27], this is computationally expensive and is not needed for the present study, where the focus lies on the CQ phase and RE formation. The ATQ methodology is designed to initiate a controlled cooling of the plasma, allowing the temperature to drop rapidly to a target level representative of post-TQ conditions. This rapid cooling mimics the TQ phase of an actual disruption, setting up the conditions necessary to study RE generation in the CQ phase. The ATQ is implemented in three subsequent key steps, described below. It is important to emphasize that this division into steps is purely intended to facilitate the simulations, addressing each aspect (thermal cooling, current flattening and impurity injection) separately.

1. Increase in thermal diffusivity: the perpendicular thermal diffusivity ($\chi_\perp$) is artificially raised to initiate a rapid temperature collapse. This step is run until the maximum electron temperature (T_e) reaches approximately 10 eV, simulating the extreme cooling that occurs during a disruption (T_e drop in Fig. 3). At the end of this step, $\chi_\perp$ is set back to its physical value (Table 1).
2. Current profile flattening: a high hyper-resistivity is applied to mimic the effects of magnetic reconnection and the current spike occurring during disruptions. This approach reduces gradients in the current density profile and flattens the safety factor (q) profile, establishing a more uniform electric field distribution (constant T_e and I_p spike in Fig. 3). During this step, the Ohmic heating is switched off in order to isolate the effect of the applied hyper-resistivity on the current profile. Once a satisfactory current profile flattening is obtained, the hyper-resistivity is set back to a negligible value.
3. Impurity injection: impurities are uniformly introduced into the computational domain. Neon is used as the impurity in the present study. Once the desired impurity level is reached, the injection is stopped. Although, physically, the injection of impurities precedes the thermal collapse, here they are not the cause of the TQ, which is triggered artificially in step 1. Impurities are instead meant to ensure a balance between the radiative cooling and Ohmic heating, in order to establish the plasma conditions that will govern the subsequent, self-consistent CQ phase, which will be run with the value of the main physical parameters reported in Table 1.

The ATQ method creates a simplified yet effective approximation of the TQ, allowing us to focus on the RE beam formation in the post-TQ phase without simulating the full complexity of the 3D TQ physics, which will be addressed in a separate work. By establishing conditions of high

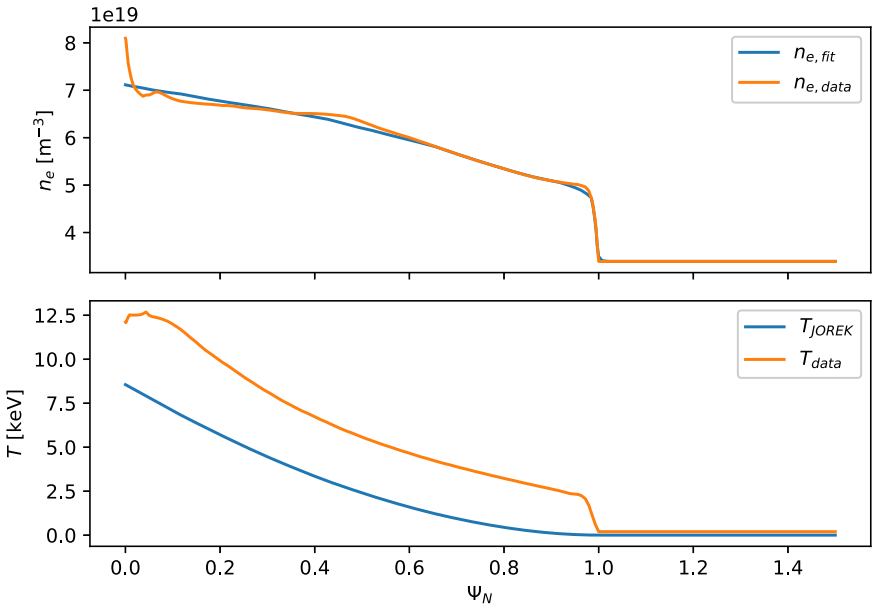

Fig. 2. Profiles of the electron density and single-fluid temperature used in this work (blue lines), compared with the profiles obtained with an older version of CREATE-NL [28] (orange lines). The density profile implemented in JOREK is a fitted approximation of the original profile. The most recent version of CREATE-NL equilibrium (blue curves, those implemented in JOREK) uses a simplified bell-shaped function for the temperature, but adopts the most up-to-date geometries and is MHD stable. The shapes of the older version (orange lines) have been plotted for reference only. The key reason why it is possible to use the simplified temperature profile is that this work focuses on the CQ (the critical phase for RE avalanche), where the temperature is a result of the self-consistent balance between Ohmic heating and impurity radiation.

resistivity and a flattened current profile, the ATQ provides a controlled environment to examine the evolution of REs in the CQ phase.

The Day-0 scenario of DTT, where the plasma current is limited to 2 MA and the vacuum toroidal magnetic field B_ϕ is limited to 3 T, provides an opportunity to evaluate RE risks in a low-power environment before advancing to higher power levels. In the framework of this study, we focus on a simplified version of the single null (SN) Day-0 scenario of DTT (scenario A1) [29], obtained with the most recent version of CREATE-NL [28], in which the temperature is assumed to follow a bell-shaped profile (blue line in Fig. 2) and the q profile is always greater than 1. For reference, Fig. 2 also depicts the non-simplified plasma temperature profile (orange curves), obtained with an older version of CREATE-NL. In this older version, the geometries were outdated and the plasma was not MHD stable. Consequently, choosing the most recent equilibrium allows us to have the most up-to-date geometries and to simplify the computation, avoiding potentially cumbersome difficulties in simulating a scenario with $q < 1$ in the core. This is possible here because, as mentioned above, during the very first step of the ATQ procedure we are numerically tuning the perpendicular thermal diffusivity in such a way as to provoke a thermal collapse. The results following this operation are marginally dependent on the initial temperature distribution, as the maximum electron temperature is decreased by several orders of magnitude ($T_{e,\max}$ in Fig. 3 goes from 4 keV to 10 eV). We want to emphasize here that the reason why it is possible to use this approach is that the focus of this work lies in the CQ phase, which is the critical one for what concerns RE multiplication. In this phase, the plasma parameters have their physical values and the temperature is calculated self-consistently according to JOREK energy balance equations. This methodology allows us to reach in a flexible and convenient way post-TQ phase, where we can focus on the CQ and RE avalanche. Additionally, in the second step of the ATQ we would have anyway a profound modification of the q profile, since it will be flattened in the core together with the plasma current profile. For this reason, considering the procedure we are carrying out within this framework, the initial conditions concerning the temperature and the q profile do not dramatically affect the results we will discuss in Section 3. The plasma density is instead obtained through a fit of the original profile to simplify numerical calculations. The temperature and plasma density as represented by the blue lines in Fig. 2 are then used inside JOREK, together with the corresponding FF' profile and the poloidal flux at the computational boundary, to calculate the initial equilibrium by solving the Grad–Shafranov equation.

As mentioned earlier, the initial RE seed used to start the simulation represents the primary RE formation mechanisms. Its estimation is challenging, as it can span several orders of magnitude. In order to provide a comprehensive assessment of the generation of REs in the Day-0 scenario of DTT, we present in Section 3 the results obtained using three different initial RE seeds: 2 A, 200 A, and 20 kA. It should be noted that this upper-bound value already represents 1% of the initial plasma current, indicating that 1% of the current after the thermal quench would be carried by electrons with kinetic energies high enough that the toroidal electric field acceleration they encounter exceeds the collisional drag. Nevertheless, it is important to examine how the change in these initial conditions affects the growth of the RE population during the CQ. Similarly, the number of impurities injected in the third step of the ATQ, as described above, is also an important factor in determining the dynamics of REs in the CQ, as they contribute to the cooling of the plasma and, hence, to the increase in electrical resistivity. Moreover, when the impurity density is large enough, the avalanche gain can be strongly boosted by the bound electrons around the partially ionized impurities, which are more efficient in increasing the avalanche growth rate by acting as knock-on targets than in reducing it by increasing drag [30]. However, unlike the initial RE seed, this parameter can be controlled externally, as the number of impurities injected inside the plasma depends on the disruption mitigation system that is used when a disruption is detected. We analyze results that span several orders of magnitude, from $N_{imp} \approx 1 \cdot 10^{19}$ to $N_{imp} \approx 3 \cdot 10^{21}$ (in a computational volume of ≈ 52 m^3). This upper-bound level indicates an impurity content which is very close to that of the background ions (Fig. 3). It is worth exploring the full range of combinations of initial RE seed and impurity content to understand to what extent the early operational phase of DTT can be considered safe with respect to REs. The parameter ranges in this work were chosen to provide a broad overview of the RE generation for this DTT scenario. Future studies

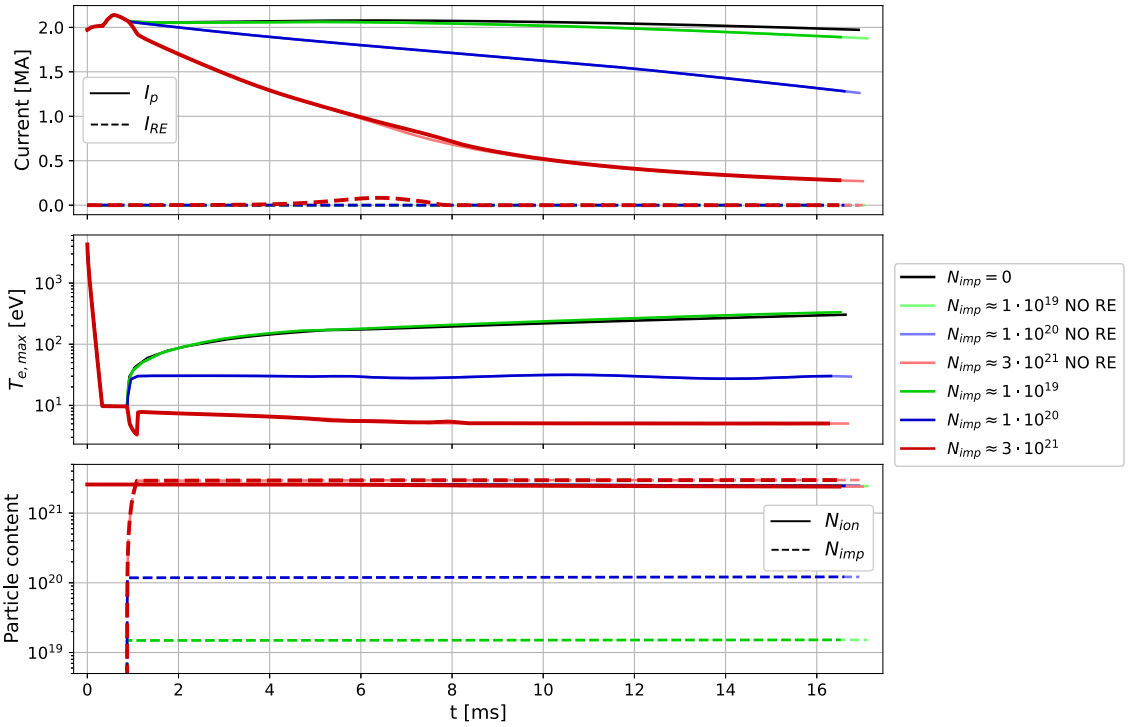

Fig. 3. From top to bottom: plasma current (I_p, solid line) and RE current (I_{RE}, dashed line); maximum electron temperature ($T_{e,max}$); particle content of ions (N_{ion}, solid line) and impurities (N_{imp}, dashed line). All the lines are drawn for different impurity levels, with and without REs under an intermediate initial RE seed current of 200 A. A brighter shade of the colors is used to indicate simulations with the same characteristics but without an RE population. For this RE seed current, they virtually superimpose with the lines for simulations that consider REs, since the role of REs is marginal in affecting the CQ dynamics here. Until $t \approx 1$ ms, all the curves overlap, since this is the phase in which the first two steps of the ATQ (as described in Section 2) are run.

may explore more pessimistic assumptions, such as higher initial seed currents and impurity concentration or different impurity species, to further probe the safety boundaries.

3. Results and discussion

This section presents and discusses the results of the simulations performed by exploring the effects of impurities and initial RE seed currents on the CQ dynamics and on the RE current growth. Several scenarios were analyzed, including a benchmark simulation with neither impurities nor REs and cases with varying impurity levels and initial RE seed currents.

Fig. 3 illustrates the disruption evolution for various levels of impurities, with and without REs, using an intermediate initial RE seed current of 200 A. The top graph shows the evolution of the plasma current (I_p, solid line) and the RE current (I_{RE}, dashed line), while the middle and bottom graphs, respectively, depict the maximum electron temperature ($T_{e,max}$) and the particle content of ions (N_{ion}, solid line) and impurities (N_{imp}, dashed line) within the computational domain. During the initial phase of the simulation, up to approximately $t \approx 1$ ms, all curves overlap. This period corresponds to the first two steps of the ATQ procedure described in Section 2. In the first step, a rapid temperature drop occurs due to the artificial increase in thermal diffusivity, reducing the electron temperature (T_e) to approximately 10 eV. In the second step, the plasma current (I_p) experiences a spike (while the electron temperature remains constant because Ohmic heating is switched off), reflecting the flattening of the current profile. The curves begin to diverge during the impurity injection phase (third step of the ATQ), as the duration of this step varies depending on the impurity content in each simulation, indicated by the color of the corresponding curve. For the case with the lowest impurity content (green line), the plasma current decays very slowly, closely resembling the benchmark case without impurities (black line). This behavior is attributed to the limited impact of impurities on the electron temperature (middle plot in Fig. 3) and, consequently, on the electrical resistivity. In contrast, higher impurity concentrations enhance radiative cooling of the plasma, maintaining a lower electron temperature during the CQ, which significantly increases plasma resistivity and accelerates the CQ, as indicated by the much more rapid decay of the plasma current (solid lines in the top plot of Fig. 3). With an initial RE seed of 200 A, the influence of REs on CQ dynamics is negligible. This is evident from the close overlap of curves with the same color but different shades in Fig. 3, corresponding to simulations with and without REs for the same impurity content. Even at the upper limit of the impurity range ($N_{imp} \approx 3 \cdot 10^{21}$), slightly exceeding the background plasma content, the maximum RE current remains below 0.1 MA.

The time evolution of plasma and RE currents resulting from simulations with the highest initial RE seed in the range considered in this work, equal to 20 kA, is shown in Fig. 4. It does not include the evolution of the maximum electron temperature and particle content, as there are virtually no differences from Fig. 3. It is immediately noticeable in Fig. 4 how this increase in the initial RE seed by a factor of 100 has changed the CQ dynamics for the simulation with the highest impurity level (the dark red curves). In fact, while a sufficiently low impurity value does not change the behavior compared to the cases without REs or with a lower RE seed, when combining the upper-bound RE seed current (20 kA) and impurity level ($3 \cdot 10^{21}$ particles), the CQ is significantly slowed by the growth of the RE current, which reaches a peak of around 0.8 MA. It could be reasonably anticipated that, in the case of strong RE formation, REs would carry the full current during the CQ at some point when the thermal current has decayed away resistively. The reason this is not the case in the scenario considered here lies in the assumed mitigation scenario and scrape-off layer (SOL) temperature. Since the dark red line in Fig. 4 corresponds to a strong injection of impurities, the post-TQ temperatures inside and outside the separatrix become comparable in the course of the CQ, so that

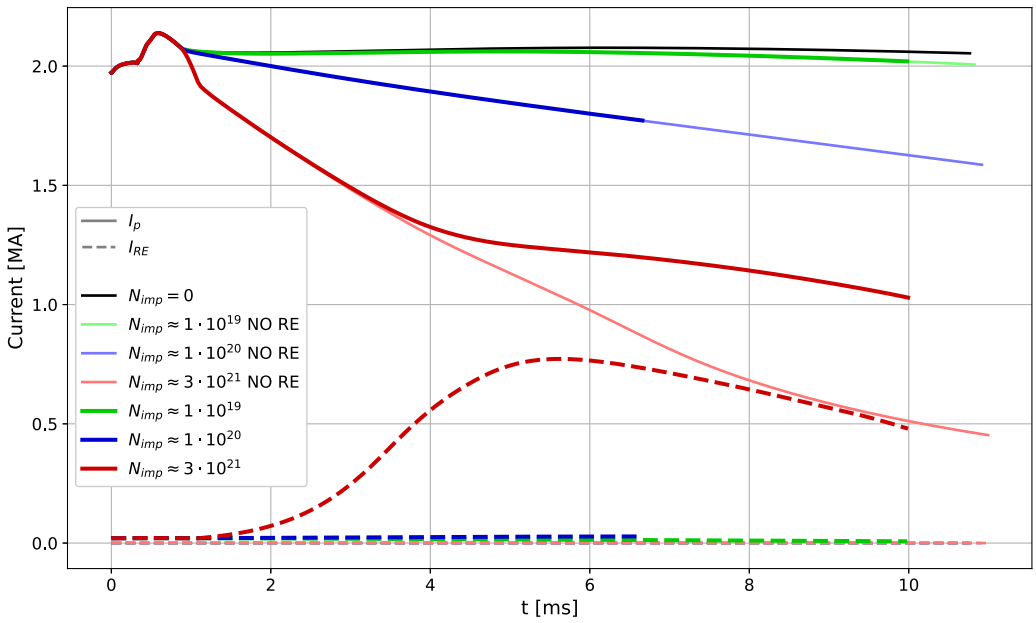

Fig. 4. Time evolution of the plasma current (I_p, solid line) and RE current (I_{RE}, dashed line) with the highest initial RE seed in the range considered in this work, equal to 20 kA. All the lines are drawn for different impurity levels, with and without REs. A lighter shade of the colors is used to indicate simulations with the same characteristics of their counterparts, but without RE population: they virtually superimpose for the two smaller impurity contents (green and blue lines), while they diverge for the highest impurity content (red lines), as REs start avalanching.

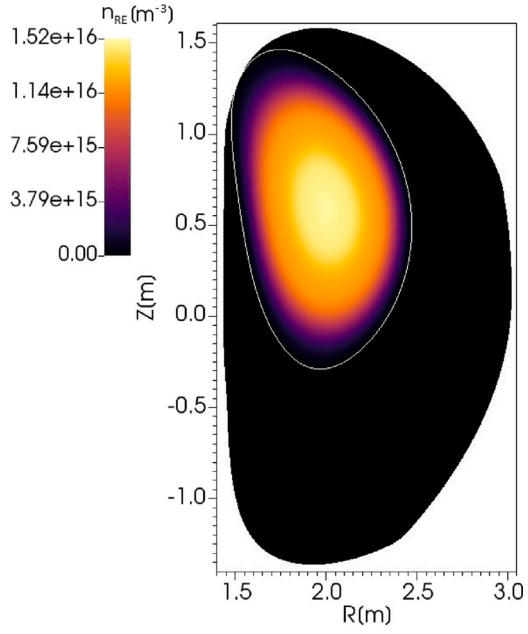

Fig. 5. RE density profile at the peak I_{RE} ($t \approx 5.7$ s) in the case with an RE seed current of 20 kA and $N_{imp} \approx 3 \cdot 10^{21}$ (dark red lines in Fig. 4). The white line indicates the separatrix and highlights the fact that all the REs are within the confined region.

substantial currents can be induced in the open field line region, as described in [26]. Moreover, the large halo currents are due to the relatively high SOL temperature during the CQ, as in these simulations it is assumed that radiation dissipation ceases below 5 eV. These currents cannot be converted into REs, as they would be immediately lost at material structures and, thus, remain thermal. Consequently, virtually the entire current inside the confined region is converted into RE current as expected, but substantial thermal currents remain in the SOL region during the vertical motion, explaining the gap between the dashed and the solid dark red lines in Fig. 4. Although the assumption on radiation dissipation does not impact the main conclusions of this paper, accurately calculating the SOL temperature will be essential for full current scenarios, where substantial RE formation is expected. Fig. 5 shows the density profile of REs at the peak of I_{RE} for the highest impurity content (dark red curve, $t \approx 5.7$ s), highlighting the fact that the growth of REs is stopped by the scraping-off of the plasma against the first wall due to its upward vertical motion.

Fig. 6 summarizes the time evolution of the RE current following different initial RE seeds and different impurity contents. For clarity, the currents corresponding to the lowest initial RE seed considered in this work (2 A) have been multiplied by 100. From the plot it is clear that the two lowest initial RE seeds, that is, 2 A and 200 A (dotted and dashed lines of Fig. 6, respectively), produce virtually the same RE current behavior, differing only by a constant scaling factor equal to the ratio of their respective initial RE seeds. The behavior is instead different when the largest initial RE seed (20 kA) is combined with the highest number of impurities: in this case, the growth of the RE current is slowed by the feedback of the electric field and by the scraping-off effect of the wall due to vertical motion (Fig. 5), limiting it to less than 1 MA. This non-linear saturation is a key result, as a 100-fold increase in the initial seed (from 200 A to 20 kA) leads to only a 10-fold increase in the maximum RE current. This suggests that our 20 kA simulation can be considered a reasonable proxy for a worst-case, avalanche-dominated scenario, at least with respect to RE seed. Were the seed an order of magnitude larger, it would constitute a significant threat on its own, even with minimal multiplication. Such a scenario would shift the focus from RE avalanche during CQ to the initial seed generation mechanisms and is outside the scope of this study.

Considering the results presented in this section, one of the key findings of this work is that non-negligible RE currents are only observed in a scenario that combines the highest initial RE seed current (20 kA) and impurity content ($N_{imp} \approx 3 \cdot 10^{21}$ particles) used in this work. In this worst-case scenario, the RE current reaches a peak of approximately 0.8 MA. Although this case highlights a scenario where REs have a noticeable impact, it is important to stress that these conditions should be easily avoidable in practical Day-0 operations of DTT. In fact, for all other combinations of initial RE seed currents and impurity levels

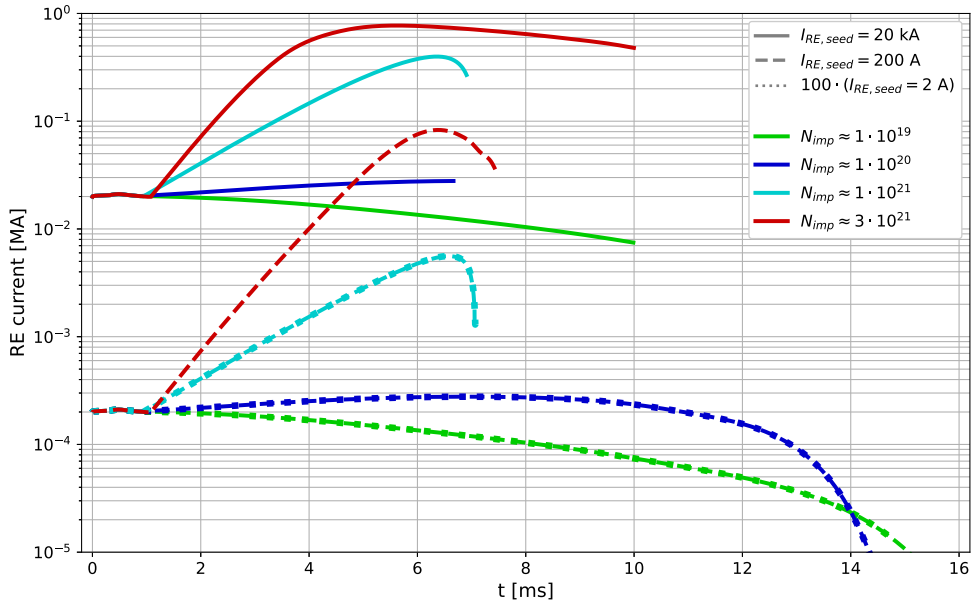

Fig. 6. Time evolution of the RE current for varying impurity levels and for the three initial RE seed currents considered in this study: 2 A (dotted lines), 200 A (dashed lines) and 20 kA (solid lines). To improve clarity, the I_{RE} values corresponding to the lowest initial seed current (2 A, dotted lines) have been scaled by a factor of 100.

studied, RE generation remains minimal to negligible. For example, with low initial RE seed currents (e.g., 2 A or 200 A), even the highest impurity levels produce RE currents well below 0.1 MA. This behavior demonstrates that under such conditions, REs do not pose a significant concern and their presence does not substantially affect CQ dynamics, as evident from the superposition of plasma current decay curves for cases with and without REs (Fig. 3). It is also worth emphasizing that the maximum value of impurity content used in some simulations was valuable for exploring the upper bounds of RE risks but does not reflect realistic operational conditions. A disruption mitigation strategy for the Day-0 phase can rely on moderate impurity injection levels, avoiding the high plasma resistivity and toroidal electric fields that favor RE generation. The results suggest that managing the number of impurities injected is a straightforward and effective approach to completely suppress RE formation. Moreover, the relatively low plasma current on Day-0 ($I_p = 2$ MA) inherently limits the RE avalanche compared to scenarios at higher current, further contributing to operational safety.

Overall, this study demonstrates that the Day-0 operational scenario of DTT can be considered safe regarding the risks associated with RE beams. With careful control of the impurity content, the generation of REs can be effectively minimized or avoided, ensuring the integrity of the plasma-facing components during this initial phase.

4. Conclusions

The investigation of RE generation in DTT during the initial Day-0 operational phase has provided valuable insights into the dynamics and risks associated with REs in a low-current setting. Using a combination of the non-linear MHD code JOREK and the vacuum-field code STARWALL, we have employed an artificial thermal quench in order to mimic the physics that occurs during a disruption, allowing us to directly simulate the current quench phase avoiding the computational complexity of self-consistent disruption simulations, which will be investigated separately in future work. This study analyzes various post-disruption conditions, obtained by systematically varying the impurity content and initial RE seed currents over several orders of magnitude, in order to evaluate their impact on RE formation. The results indicate that in the Day-0 scenario, where plasma current is limited to 2 MA, it is possible to observe relatively high RE beam currents (≈ 0.8 MA) only when an initial RE seed current of 20 kA, the upper bound of our scan, is combined with an impurity content slightly larger than that of the background plasma. Even if it is difficult to predict with confidence the magnitude of the initial RE seed current, it is possible to design a disruption mitigation strategy for the Day-0 scenario that does not require the injection of such a large number of impurity particles, thus avoiding the conditions that dramatically enhance the RE avalanche in the first place. These findings underscore how, at reduced power levels, REs pose minimal risks to the plasma-facing components of DTT, confirming the safety regarding REs during the Day-0 phase and removing the immediate need for complex RE mitigation strategies. It is important to emphasize that this work is specifically limited to the risks associated with runaway electron generation in the DTT Day-0 scenario. A comprehensive disruption safety assessment must also consider other critical aspects, such as the thermal loads on PFCs during the TQ and electromagnetic forces. Such an integrated analysis is beyond the scope of the present study.

As DTT transitions to full power scenarios, with target plasma currents up to 5.5 MA, the potential for RE generation and the associated risks to PFCs will increase. The Day-0 scenario is not easily susceptible to RE formation (except for the pessimistic case combining the upper ends of our parameter scan), since the RE avalanching is not fast enough in comparison to the vertical motion of the plasma. Dedicated RE studies for DTT 2 MA operation would likely only be realistic in circular plasma cross-sections, where no vertical instability arises, and an RE beam can form on longer timescales. However, as the operation scales up to full power (5.5 MA), the RE avalanche is expected to accelerate significantly due to its exponential dependence on the pre-disruption current. Consequently, the maximum potential avalanching gain will increase substantially, making RE formation a much more critical concern in standard elongated configurations, highlighting the need for further investigations.

Future studies will focus on examining RE behavior in DTT's 5.5 MA scenario, including the investigation of mitigation strategies such as the strategic placement of sacrificial limiters to protect the first wall from the elevated RE loads anticipated at higher currents. Furthermore, incorporating 3D plasma instabilities and dynamics, as well as assessing detailed 3D RE termination events, will provide a more comprehensive understanding of RE beam dynamics and their interaction with PFCs. These efforts will yield critical insights, ensuring RE-safe operation of DTT and enabling its role as a valuable platform for advancing fusion energy research and technology development.

CRediT authorship contribution statement

Enrico Emanuelli: Writing – review & editing, Writing – original draft, Visualization, Validation, Software, Methodology, Investigation, Formal analysis, Data curation, Conceptualization. **Francesco Vannini:** Writing – review & editing, Supervision, Software, Methodology, Conceptualization. **Matthias Hoelzl:** Writing – review & editing, Supervision, Software, Resources, Project administration, Methodology, Conceptualization. **Nina Schwarz:** Writing – review & editing, Software, Methodology, Conceptualization. **Eric Nardon:** Writing – review & editing, Supervision, Software, Methodology, Conceptualization. **Vinodh Bandaru:** Writing – review & editing, Supervision, Software, Methodology, Conceptualization. **Daniele Bonfiglio:** Writing – review & editing, Supervision, Software, Project administration, Methodology, Conceptualization. **Artur Kryzhanovskyy:** Writing – review & editing, Methodology. **Giuseppe Ramogida:** Writing – review & editing, Supervision, Project administration, Conceptualization. **Fabio Subba:** Writing – review & editing, Supervision, Project administration, Conceptualization.

Declaration of competing interest

The authors declare that they have no known competing financial interests or personal relationships that could have appeared to influence the work reported in this paper.

Acknowledgments

This work has been carried out within the framework of the EUROfusion Consortium, funded by the European Union via the Euratom Research and Training Programme (Grant Agreement No 101052200 — EUROfusion). Views and opinions expressed are however those of the author(s) only and do not necessarily reflect those of the European Union or the European Commission. Neither the European Union nor the European Commission can be held responsible for them. The simulations were performed on the Marconi-Fusion supercomputer hosted at CINECA.

Data availability

Data will be made available on request.

References

[1] ITER Physics Expert Group on Disruptions and Plasma Control and MHD, ITER Physics Basis Editors, Chapter 3: MHD stability, operational limits and disruptions, Nucl. Fusion 39 (12) (1999) 2251, http://dx.doi.org/10.1088/0029-5515/39/12/303.

[2] T.C. Hender, J.C. Wesley, J. Bialek, A. Bondeson, A.H. Boozer, R.J. Buttery, A. Garofalo, T.P. Goodman, R.S. Granetz, Y. Gribov, O. Gruber, M. Gryaznevich, G. Giruzzi, S. Günter, N. Hayashi, P. Helander, C.C. Hegna, D.F. Howell, D.A. Humphreys, G.T.A. Huysmans, A.W. Hyatt, A. Isayama, S.C. Jardin, Y. Kawano, A. Kellman, C. Kessel, H.R. Koslowski, R.J.L. Haye, E. Lazzaro, Y.Q. Liu, V. Lukash, J. Manickam, S. Medvedev, V. Mertens, S.V. Mirnov, Y. Nakamura, G. Navratil, M. Okabayashi, T. Ozeki, R. Paccagnella, G. Pautasso, F. Porcelli, V.D. Pustovitov, V. Riccardo, M. Sato, O. Sauter, M.J. Schaffer, M. Shimada, P. Sonato, E.J. Strait, M. Sugihara, M. Takechi, A.D. Turnbull, E. Westerhof, D.G. Whyte, R. Yoshino, H. Zohm, the ITPA MHD, Disruption, Magnetic Control Topical Group, Chapter 3: MHD stability, operational limits and disruptions, Nucl. Fusion 47 (6) (2007) S128, http://dx.doi.org/10.1088/0029-5515/47/6/S03.

[3] ITER Physics Basis Editors, ITER Physics Expert Group Chairs and Co-Chairs, ITER Joint Central Team and Physics Integration Unit, Chapter 1: Overview and summary, Nucl. Fusion 39 (12) (1999) 2137, http://dx.doi.org/10.1088/0029-5515/39/12/301.

[4] G. Federici, C. Bachmann, L. Barucca, C. Baylard, W. Biel, L.V. Boccaccini, C. Bustreo, S. Ciattaglia, F. Cismondi, V. Corato, C. Day, E. Diegele, T. Franke, E. Gaio, C. Gliss, T. Haertl, A. Ibarra, J. Holden, G. Keech, R. Kembleton, A. Loving, F. Maviglia, J. Morris, B. Meszaros, I. Moscato, G. Pintsuk, M. Siccinio, N. Taylor, M.Q. Tran, C. Vorpahl, H. Walden, J.H. You, Overview of the DEMO staged design approach in Europe, Nucl. Fusion 59 (6) (2019) 066013, http://dx.doi.org/10.1088/1741-4326/ab1178, Publisher: IOP Publishing.

[5] N. Schwarz, F.J. Artola, F. Vannini, M. Hoelzl, M. Bernert, A. Bock, T. Driessen, M. Dunne, L. Giannone, P. Heinrich, P.d. Marné, G. Papp, G. Pautasso, S. Gerasimov, the ASDEX Upgrade Team, J. E. T. Contributors, Team the JOREK, The mechanism of the global vertical force reduction in disruptions mitigated by massive material injection, Nucl. Fusion 63 (12) (2023) 126016, http://dx.doi.org/10.1088/1741-4326/acf50a, Publisher: IOP Publishing.

[6] A.H. Boozer, Pivotal issues on relativistic electrons in ITER, Nucl. Fusion 58 (3) (2018) 036006, http://dx.doi.org/10.1088/1741-4326/aaa1db, Publisher: IOP Publishing.

[7] B.N. Breizman, P. Aleynikov, E.M. Hollmann, M. Lehnen, Physics of runaway electrons in tokamaks, Nucl. Fusion 59 (8) (2019) 083001, http://dx.doi.org/10.1088/1741-4326/ab1822, Publisher: IOP Publishing.

[8] G.F. Matthews, B. Bazylev, A. Baron-Wiechec, J. Coenen, K. Heinola, V. Kiptily, H. Maier, C. Reux, V. Riccardo, F. Rimini, G. Sergienko, V. Thompson, A. Widdowson, J. E. T. Contributors7, Melt damage to the JET ITER-like Wall and divertor, Phys. Scr. 2016 (2016) 014070, http://dx.doi.org/10.1088/0031-8949/T167/1/014070, Publisher: IOP Publishing.

[9] C. Reux, V. Plyusnin, B. Alper, D. Alves, B. Bazylev, E. Belonohy, A. Boboc, S. Brezinsek, I. Coffey, J. Decker, P. Drewelow, S. Devaux, P.C.d. Vries, A. Fil, S. Gerasimov, L. Giacomelli, S. Jachmich, E.M. Khilkevitch, V. Kiptily, R. Koslowski, U. Kruezi, M. Lehnen, I. Lupelli, P.J. Lomas, A. Manzanares, A.M.D. Aguilera, G.F. Matthews, J. Mlynář, E. Nardon, E. Nilsson, C.P.v. Thun, V. Riccardo, F. Saint-Laurent, A.E. Shevelev, G. Sips, C. Sozzi, J. E. T. contributors, Runaway electron beam generation and mitigation during disruptions at JET-ILW, Nucl. Fusion 55 (9) (2015) 093013, http://dx.doi.org/10.1088/0029-5515/55/9/093013, Publisher: IOP Publishing.

[10] R. Martone, R. Albanese, F. Crisanti, P. Martin, A. Pizzuto, Divertor tokamak test facility interim design report, 2019, ENEA, URL www.dtt-project.it/DTT_IDR_2019_WEB.pdf.

[11] F. Romanelli, o.b.o.D. Contributors, D. Abate, E. Acampora, D. Agguiaro, R. Agnello, P. Agostinetti, M. Agostini, A. Aimetta, R. Albanese, G. Alberti, M. Albino, E. Alessi, S. Almaviva, M. Alonzo, R. Ambrosino, P. Andreoli, M. Angelone, M. Angelucci, C. Angioni, A.A. Armenio, P. Antonini, D. Aprile, G. Apruzzese, M. Aquilini, G. Aragone, P. Arena, M. Ariola, G. Artaserse, L. Aucone, A. Augieri, F. Auriemma, J.A. Guerola, N. Badodi, B. Baiocchi, L. Balbinot, C. Baldacchini, A. Balestri, T. Barberis, G. Barone, L. Barucca, M. Baruzzo, S. Begozzi, V. Belardi, F. Belli, A. Belpane, F. Beone, S. Bertolami, S. Bianucci, S. Bifaretti, S. Bigioni, W. Bin, P. Boccali, B. Boeswirth, E. Bogazzi, R. Bojoi, S. Bollanti, T. Bolzonella, F. Bombarda, M. Bonan, N. Bonanomi, A. Bonaventura, L. Boncagni, M. Bonesso, D. Bonfiglio, R. Bonifetto, D. Bonomi, D. Borgogno, T. Borzone, S. Botti, E. Boz, F. Braghin, M. Brena, S. Brezinsek, M. Brombin, A. Bruschi, S. Buonocore, P. Buratti, P. Buratti, D. Busi, G. Calabrò, M. Caldora, G. Calvo, G. Camera, G. Campana, S. Candela, V. Candela, F. Cani, L. Cantone, F. Capaldo, S. Cappello, M. Caponero, S. Carchella, A. Cardinali, D. Carnevale, L. Carraro, C. Carrelli, V. Casalegno, I. Casiraghi, C. Castaldo, A. Castaldo, G. Castro, A. Carpignano, F. Causa, R. Cavazzana, M. Cavedon, M. Cavenago, M. Cecchini, S. Ceccuzzi, G. Celentano, L. Celona, C. Centioli, G.V. Centomani, S. Cesaroni, A.G. Chiariello, R. Chomicz, C. Cianfarani, F. Cichocki, M. Cinque, A. Cioffi, M. Ciotti, M. Cipriani, S. Ciufo, V. Claps, G. Claps, V. Coccorese, D. Coccorese, A. Colangeli, T. Coltella, F. Consoli, F. Cordella, D. Corradini, O. Costa, F. Crea, A. Cremona, F. Crescenzi, F. Crisanti, G. Cristofari, G. Croci, A. Cucchiaro, D. D'Ambrosio, M.D. Molin, M.D. Palma, F. Danè, C. Day, M.D. Angeli, V.D. Leo, R.D. Luca, E.D. Marchi, G.D. Marzi, G.D. Masi, E.D. Nardi, C.D. Piccoli, G.D. Sano, M.D. Santis, G.D. Tommasi, A.D. Nevo, A. Delfino, A.D. Corte, P. Deodati, S. Desiderati, E.D. Ferdinando, M.G.D. Florio, G.D. Gironimo, L.E.D. Grazia, V.D. Marzo, F.D. Paolo, E.D. Pietro, M.D. Pietrantonio, M.D. Prinzio, A.D. Silvestre, A.D. Zenobio, R. Dima, A. Domenichelli, A. Doria, G. Dose, S. Dubbioso, S. Dulla, I. Duran, M. Eboli, M. Elitropi, E. Emanuelli, B. Esposito, P. Ettorre, C. Fabbri, F. Fabbri, M. Fadone, M.M. Faggiano, F. Falcioni, M.V. Falessi, F. Fanale, P. Fanelli, A. Fassina, A. Fassina, M. Favaretto, G. Favero, M. Ferraris, F. Ferrazza, C. Ferretti, A. Ferro, N. Ferron, C.F. Zignani, L. Figini, F. Filippi, M. Filippini, A. Fimiani, M. Fincato, F. Fiorenza, D. Fiorucci, D. Flammini, F. Flora, N. Fonnesu, P. Franz, L. Frassinetti, A. Frattolillo, R. Freda, R. Fresa, A. Frescura, P. Frosi, M. Fulici, M.F. Palumbo, V. Fusco, P. Fusco, L. Gabellier, P. Gaetani, E. Gaio, E. Gajetti, P. Gaetani, A. Galatà, J.G. Quiroga, D.L.G. Huertas, S. Gammino, G. Gandolfo, S. Garavaglia, J.G. Lopez, M.G. Muñoz, P. Gaudio, M. Gelfusa, G. Gervasini, L. Giannini, M. Giarrusso, C. Gil, F. Giorgetti, E. Giovannozzi, G. Giruzzi, L. Giudicotti, M. Gobbin, G. Gorini, G. Granucci, D. Grasso, T. Grasso, S. Grazioso, H. Greuner, G. Griva, G. Grosso, S. Guerini, J.P. Gunn, V. Hauer, J.H. Salaverri, M. Hoppe, M. Houry, M. Hoelzl, A. Iaboni, M. Iafrati, A. Iaiunese, V. Imbriani, D. Indrigo, P. Innocente, F. Koechl, B. Končar, A. Kryzhanovskyy, L. Laguardia, D.A. Lampasi, C. Lanchi, F. Lanzotti, A. Lanzotti, M. Laquaniti, F. Leone, J. Li, M. Libè, F. Lisanti, D. Liuzza, F. Locati, R. Lombroni, R. Lorenzini, P. Lorusso, L. Lotto, J. Loureiro, F. Lucca, T.L.D. Cortemiglia, P. Maccari, G. Maddaluno, S. Magagnino, G. Manca, A. Mancini, P. Mandalà, B. Mandolesi, F. Mandrile, G. Manduchi, S. Manfrin, M. Manganelli, P. Mantica, G. Marchiori, N. Marconato, G. Marelli, A. Mariani, A. Marin, R. Marinari, M. Marinelli, F. Marino, P. Marino, D. Marocco, R. Marsilio, E. Martelli, P. Martin, F. Martinelli, G. Martini, R. Martone, A. Marucci, D. Marzullo, V. Masala, D. Mascali, F. Mascari, A. Masi, N. Massanova, S. Mastrostefano, M. Mattei, G. Mauro, S. Mauro, C.

Meineri, L. Melaragni, A. Mele, P. Meller, S. Meloni, I. Menicucci, G. Messina, L. Mezi, G. Miccichè, M. Micheletti, S. Migliori, D. Milanesio, F. Milazzo, R. Milazzo, P. Minelli, S. Minucci, F. Mirizzi, M. Missirlian, D. Monarca, C. Monti, M. Mori, A. Moriani, L. Morici, A. Moro, A. Moro, F. Moro, P. Mosetti, R. Mozzillo, A. Murari, A. Muraro, D. Murra, P. Muscente, S. Musumeci, L. Muzzi, G.F. Nallo, F. Napoli, E. Nardon, E. Naselli, R. Neu, M. Nocente, M. Notazio, S. Nowak, E. Ocello, A. Oliva, V. Orsetti, A. Orsini, F.P. Orsitto, M. Ortino, M. Ottavi, G. Paccagnella, D. Pacella, I. Pagani, N. Paganucci, A. Pagliaro, V. Palazzolo, M. Palermo, S. Palomba, F. Panza, D. Paoletti, M. Parisi, R. Pasqualotto, S. Passarello, M. Passoni, T. Patton, L. Pelliccia, A. Peloso, A. Pepato, E. Perelli, A. Perencin, S. Peruzzo, A. Pesenti, N. Pedroni, P. Petrolini, V. Piergotti, A. Pidatella, L. Pigatto, M. Pillon, T. Pinna, S. Pipolo, S. Piras, C. Piron, L. Piron, A. Pironti, M. Pistilli, D. Placido, A. Pizzuto, P. Platania, A. Polimadei, F. Pollastrone, G.M. Polli, N. Pomaro, F. Pompili, C. Ponti, F. Porcelli, V. Prandelli, A. Previti, A. Princiotta, G. Pucino, F. Quaglia, A. Quercia, F. Raffaelli, G. Ramogida, G. Ranieri, B. Raspante, D. Ravarotto, G.L. Ravera, A. Reale, P. Rebesan, M. Recchia, D. Regine, F. Renno, B. Riccardi, D. Ricci, D. Rigamonti, M. Ripani, N. Rispoli, S. Roccella, G. Rocchi, H. Roche, M. Romanato, F. Romanelli, F. Romanelli, G. Romanelli, R. Romaniello, A. Romano, M. Romano, R. Romano, R. Rossi, G. Rubinacci, G. Rubino, G. Rubino, S. Rubino, J.R. Rueda, A. Rufoloni, C. Salvia, P. Salvini, M. Scarpari, A. Salvitti, L. Salvò, S. Sandri, F. Santoro, A. Satriano, L. Savoldi, C. Scardino, G. Schettini, S. Schmuck, J. Scionti, M. Scisciò, M. Scungio, K. Sedlak, L. Senni, G. Sias, A. Sibio, A. Simonetto, L. Singh, A. Sirignano, C. Sozzi, I. Spada, S. Spagnolo, L. Spinicci, G. Spizzo, M. Spolaore, C. Stefanini, H. Strobel, F. Subba, F. Taccogna, B. Taheri, C. Tantos, A. Tarallo, M. Tarantino, G. Tardini, M. Tardocchi, P. Tarfila, A. Tenaglia, C. Terlizzi, D. Terranova, D. Testa, E. Testa, R. Testoni, V. Toigo, G. Torrisi, A. Trotta, G. Trovato, E. Tsitrone, A. Tuccillo, O. Tudisco, M. Turcato, S. Turtù, A. Uccello, M. Ugoletti, O. Uras, M. Uras, M. Utili, V. Vaccaro, F. Valentini, L. Valletti, M. Valisa, D.V. Eester, D. Vanzan, E. Vassallo, G. Vecchi, M. Vellucci, I. Venneri, G. Ventura, M. Veranda, L. Verdini, C. Verona, G.V. Rinati, F. Veronese, N. Vianello, F. Viganò, O. Villano, R. Villari, F. Villone, P. Vincenzi, V. Vitale, F. Vivio, G. Vlad, M. Wischmeier, H.S. Wu, I. Wyss, R. Zanino, B. Zaniol, F. Zanon, A. Zappatore, G. Zavarise, P. Zito, A. Zoppoli, M. Zucchetti, M. Zuin, P. Zumbolo, Divertor Tokamak Test facility project: status of design and implementation, Nucl. Fusion 64 (11) (2024) 112015, http://dx.doi.org/10.1088/1741-4326/ad5740, Publisher: IOP Publishing.

[12] M. Hoelzl, G.T.A. Huijsmans, S.J.P. Pamela, M. Bécoulet, E. Nardon, F.J. Artola, B. Nkonga, C.V. Atanasiu, V. Bandaru, A. Bhole, D. Bonfiglio, A. Cathey, O. Czarny, A. Dvornova, T. Fehér, A. Fil, E. Franck, S. Futatani, M. Gruca, H. Guillard, J.W. Haverkort, I. Holod, D. Hu, S.K. Kim, S.Q. Korving, L. Kos, I. Krebs, L. Kripner, G. Latu, F. Liu, P. Merkel, D. Meshcheriakov, V. Mitterauer, S. Mochalskyy, J.A. Morales, R. Nies, N. Nikulsin, F. Orain, J. Pratt, R. Ramasamy, P. Ramet, C. Reux, K. Särkimäki, N. Schwarz, P.S. Verma, S.F. Smith, C. Sommariva, E. Strumberger, D.C.v. Vugt, M. Verbeek, E. Westerhof, F. Wieschollek, J. Zielinski, The JOREK non-linear extended MHD code and applications to large-scale instabilities and their control in magnetically confined fusion plasmas, Nucl. Fusion 61 (6) (2021) 065001, http://dx.doi.org/10.1088/1741-4326/abf99f, Publisher: IOP Publishing.

[13] M. Hoelzl, G.T.A. Huijsmans, F.J. Artola, E. Nardon, M. Becoulet, N. Schwarz, A. Cathey, S.J.P. Pamela, K. Aleynikova, F. Antlitz, V. Bandaru, H. Bergström, A. Bhole, T. Bogaarts, D. Bonfiglio, F. Cipolletta, T. Driessen, L. Edes, S. Futatani, G. Hao, F. Hindenlang, I. Holod, D. Hu, S. Hu, N. Isernia, H. Isliker, S.K. Kim, M. Kong, S. Korving, L. Kos, I. Krebs, S.J. Lee, Y.C. Liang, Z. Liang, S.J. Liu, Z.X. Lu, L. Meier, L. Messfeldt, V. Mitterauer, N. Nikulsin, B. Nkonga, R. Ramasamy, J. Reinking, C. Rogge, G. Rubinacci, K. Särkimäki, T. Smits, C. Sommariva, R. Sparago, K. Strien, M. Szucs, W. Tang, J.v. Tongeren, F. Vannini, S. Ventre, F. Villone, C. Wang, L. Wang, F. Wieschollek, F. Wouters, J. Zielinski, H. Zhang, Non-linear MHD modelling of transients in tokamaks: a review of recent advances with the JOREK code, Nucl. Fusion 64 (11) (2024) 112016, http://dx.doi.org/10.1088/1741-4326/ad5a21, Publisher: IOP Publishing.

[14] P. Merkel, E. Strumberger, Linear MHD stability studies with the STARWALL code, 2015, arXiv:1508.04911, URL https://arxiv.org/abs/1508.04911.

[15] M. Hoelzl, P. Merkel, G.T.A. Huysmans, E. Nardon, E. Strumberger, R. McAdams, I. Chapman, S. Günter, K. Lackner, Coupling JOREK and STARWALL codes for non-linear resistive-wall simulations, J. Phys.: Conf. Ser. 401 (1) (2012) 012010, http://dx.doi.org/10.1088/1742-6596/401/1/012010.

[16] O. Czarny, G. Huysmans, Bézier surfaces and finite elements for MHD simulations, J. Comput. Phys. 227 (16) (2008) 7423–7445, http://dx.doi.org/10.1016/j.jcp.2008.04.001.

[17] V. Bandaru, M. Hoelzl, F.J. Artola, G. Papp, G.T.A. Huijsmans, Simulating the nonlinear interaction of relativistic electrons and tokamak plasma instabilities: Implementation and validation of a fluid model, Phys. Rev. E 99 (2019) 063317, http://dx.doi.org/10.1103/PhysRevE.99.063317, URL https://link.aps.org/doi/10.1103/PhysRevE.99.063317.

[18] M.N. Rosenbluth, S.V. Putvinski, Theory for avalanche of runaway electrons in tokamaks, Nucl. Fusion 37 (10) (1997) 1355, http://dx.doi.org/10.1088/0029-5515/37/10/I03.

[19] V. Bandaru, M. Hoelzl, F.J. Artola, O. Vallhagen, M. Lehnen, JOREK Team, Runaway electron fluid model extension in JOREK and ITER relevant benchmarks, Phys. Plasmas 31 (8) (2024) 082503, http://dx.doi.org/10.1063/5.0213962.

[20] V. Bandaru, M. Hoelzl, C. Reux, O. Ficker, S. Silburn, M. Lehnen, N. Eidietis, J. Team, J.E.T. Contributors, Magnetohydrodynamic simulations of runaway electron beam termination in JET, Plasma Phys. Control. Fusion 63 (3) (2021) 035024, http://dx.doi.org/10.1088/1361-6587/abdbcf, Publisher: IOP Publishing.

[21] V. Bandaru, M. Hoelzl, H. Bergström, F.J. Artola, K. Särkimäki, M. Lehnen, the JOREK Team, Assessment of runaway electron beam termination and impact in ITER, Nucl. Fusion 64 (7) (2024) 076053, http://dx.doi.org/10.1088/1741-4326/ad50ea, Publisher: IOP Publishing.

[22] H. Bergström, K. Särkimäki, V. Bandaru, M.M. Skyllas, M. Hoelzl, JOREK Team, Assessment of the runaway electron load distribution in ITER during 3D MHD induced beam termination, Plasma Phys. Control. Fusion 66 (9) (2024) 095001, http://dx.doi.org/10.1088/1361-6587/ad5fb5, Publisher: IOP Publishing.

[23] V. Bandaru, M. Hoelzl, F.J. Artola, M. Lehnen, JOREK team, Axisymmetric predictions for mitigated and vertically unstable disruptions in ITER with runaway electrons, J. Plasma Phys. 91 (1) (2025) E27, http://dx.doi.org/10.1017/S0022377824001661.

[24] C. Wang, E. Nardon, F.J. Artola, V. Bandaru, M. Hoelzl, the JOREK team, The effect of vertical displacements on the runaway electron avalanche in ITER mitigated disruptions, Nucl. Fusion 65 (1) (2024) 016012, http://dx.doi.org/10.1088/1741-4326/ad8d66, Publisher: IOP Publishing.

[25] F. Vannini, V. Bandaru, H. Bergström, N. Schwarz, F.J. Artola, M. Hoelzl, G. Pautasso, E. Nardon, F. Maviglia, M.L. Richiusa, E. Emanuelli, the JOREK team, Runaway electron beam formation, vertical motion, termination and wall loads in EU-DEMO, Nucl. Fusion 65 (4) (2025) 046006, http://dx.doi.org/10.1088/1741-4326/adac77, Publisher: IOP Publishing.

[26] N. Schwarz, F.J. Artola, M. Hoelzl, M. Bernert, D. Brida, L. Giannone, M. Maraschek, G. Papp, G. Pautasso, B. Sieglin, I. Zammuto, the ASDEX Upgrade Team, the JOREK team, Experiments and non-linear MHD simulations of hot vertical displacement events in ASDEX-Upgrade, Plasma Phys. Control. Fusion 65 (5) (2023) 054003, http://dx.doi.org/10.1088/1361-6587/acc358, Publisher: IOP Publishing.

[27] S.L. Hu, D. Hu, J.Q. Li, G.Z. Hao, Y.B. Dong, G. Huijsmans, JOREK Team, Magnetohydrodynamic features and particle transport during thermal quench in HL-2A with density source, Phys. Plasmas 30 (11) (2023) 112509, http://dx.doi.org/10.1063/5.0163120.

[28] R. Albanese, R. Ambrosino, M. Mattei, CREATE-NL+: A robust control-oriented free boundary dynamic plasma equilibrium solver, SOFT-28, in: Proceedings of the 28th Symposium On Fusion Technology, vol. 96–97, 2015, pp. 664–667, http://dx.doi.org/10.1016/j.fusengdes.2015.06.162.

[29] I. Casiraghi, P. Mantica, R. Ambrosino, L. Aucone, B. Baiocchi, L. Balbinot, T. Barberis, A. Castaldo, M. Cavedon, L. Frassinetti, P. Innocente, F. Koechl, S. Nowak, P. Agostinetti, S. Ceccuzzi, L. Figini, G. Granucci, P. Vincenzi, Core integrated simulations for the Divertor Tokamak Test facility scenarios towards consistent core-pedestal-SOL modelling, Plasma Phys. Control. Fusion 65 (3) (2023) 035017, http://dx.doi.org/10.1088/1361-6587/acb6b1, Publisher: IOP Publishing.

[30] L. Hesslow, O. Embréus, O. Vallhagen, T. Fülöp, Influence of massive material injection on avalanche runaway generation during tokamak disruptions, Nucl. Fusion 59 (8) (2019) 084004, http://dx.doi.org/10.1088/1741-4326/ab26c2, Publisher: IOP Publishing.